Epikarst control on flow and storage at James Cave, VA: an analog for water resource characterization in Shenandoah Valley karst

Jonathan Daniel Gerst

Thesis submitted to the faculty of the Virginia Polytechnic Institute and State University
in partial fulfillment of the requirements for the degree of

Master of Science
In
Geosciences

Madeline E. Schreiber
Benjamin F. Schwarz
J. Donald Rimstidt
Tom J. Burbey

07/12/2010
Blacksburg, Virginia

Keywords: epikarst, karst aquifer, groundwater, watershed management

Epikarst control on flow and storage at James Cave, VA:
an analog for water resource characterization in Shenandoah Valley karst

Jonathan Daniel Gerst

ABSTRACT

Karst aquifers host significant water supplies but are easily contaminated because highly conductive inlets can rapidly transmit water to depth. The epikarst, which is the region of vegetation, soil, and weathered bedrock above karst aquifers, is a critical zone as it regulates the quantity and quality of recharge to the aquifer. As the epikarst exhibits complex heterogeneity, characterization at the field scale can be challenging. The objective of this thesis was to develop a model of epikarst hydrodynamics using long-term field measurements. To meet this objective, continuous hydrologic data of precipitation, speleothem drips, and an underground stream in James Cave in Pulaski County, VA, were collected to delineate seasonal recharge patterns, estimate effective recharge and catchment areas, characterize the number and permeability of flow paths, and evaluate storativity in the epikarst.

Results demonstrate that after significant seasonal recharge, which occurs in the late winter and early spring, the epikarst can temporarily store a significant portion of recharge in low permeability flow paths. Effective recharge was estimated to be approximately 30% of total precipitation (2008-2009). Hydrograph recession analysis aided in delineation of flowpaths in the epikarst, including quickflow, moderate flow, and baseflow components. Hydrograph shape analysis suggests flow restrictions at two of the drip sites that may reveal spatial differences in storage capacity and retention time. Results of this work are intended to aid karst aquifer management by providing a multi-technique approach that can be used to assess seasonal patterns of recharge, quantify flowpath and storage characteristics, and delineate recharge zones.

ACKNOWLEDGEMENTS

I would like to thank the National Institute for Water Resources, the Virginia Water Resources Research Center, the Cave Conservancy of the Virginias, the Geosciences Department at Virginia Tech, the Virginia Tech Graduate School, and the Geological Society of America for providing funding for research and travel to conferences. I would also like to thank the Virginia Polytechnic Institute Grotto and the Geosciences Department at Virginia Tech for providing an excellent community of field and lab volunteers. I am especially appreciative of my collaborators at the Virginia Department of Conservation of Recreation (DCR), the United States Geologic Survey (USGS), Texas State University San Marcos (TSU), American University (AU), and Virginia Tech (VT).

I would like to thank Wil Orndorff (DCR) for helping me to manage land access issues in spite of regional cave closures due to White Nose Syndrome, and also for carrying on with data collection after my graduation. In particular, Maddy Schreiber (VT), Benjamin Schwartz (TSU), Dan Doctor (USGS), and Wil Orndorff have provided invaluable assistance in helping to instrument the cave, troubleshoot equipment malfunctions, assist with sample analysis, develop my analytical methods, and most importantly, for providing critical peer review in a constructive manner. Maddy, Ben, Wil, and Dan; I am incredibly appreciative of all your hard work and support, and can't imagine working with a better team of scientists. I hope that one day I too can provide a young mind with the wisdom and zeal for learning that you all have so graciously imparted to me.

I owe tremendous thanks to the Ferrell family for cave access. I also owe thanks to David Culver and Janet Reid for assisting with biological sampling and analysis. Tom Malabad has provided a great service to the project by donating time and survey equipment to characterize epikarst thickness and station orientation. J.P. Gannon has provided direction and assistance with Electrical Resistivity Tomography (ERT) surveys by using ERT equipment that was loaned to the project by Tom Burbey of the Geosciences Department at Virginia Tech. I would also like to thank Heather Scott, Ariel Brown, Nathan Farrar, Sally Morgan, and Stuart Hyde for assisting with field work, and maintaining a superior level of diligence in data collection, even in my absence. I would also like to thank Yinka Oyewumi, Denise Levitan, Anna Hardy, and Athena Tilley for providing excellence in sample analysis. I also owe Jim Langridge and David West many thanks for fixing all of my computer woes for free and without fuss.

I would like to thank Bill Anderson, Ellen Cowan, Loren Raymond, and Scott McDowell for encouraging me to pursue graduate study and putting me on a career path that I truly love and can believe in. I would also like to thank Desiree Staires, Robert Burke, J.P. Gannon, Phil Prince, and Yinka Oyewumi for not only providing critical peer review, but also providing friendships that I hope will last a lifetime. Last, I owe my wife, Alexandra Gerst, and my parents, Daniel and Tari Gerst, congratulations and several thanks for their support and encouragement. Even during hard times, you all have provided unconditional love and unparalleled support. Your presence in my life means the world to me, and will always give me a reason to return home after a hard days adventure! I am forever indebted to all of the aforementioned individuals because it was through our combined efforts that we were able to make this project a success.

Table of Contents

List of Tables

List of Figures

1. INTRODUCTION

Karst aquifers are unique groundwater reservoirs that provide significant amounts of water. It is estimated that karst aquifers supply the United States with 40% of its drinking water, and that more than 25% of the world's population lives on or obtains its water from karst aquifers (KWI, 2003). Although karst aquifers host significant water supplies, they are easily contaminated because the predominant recharge mechanism to the aquifer is fast flow through open conduits and fractures (sometimes to great depths) that have been enlarged by chemical dissolution. Population growth, urban development, and agriculture are increasing demands while also increasing contamination of these sensitive water resources. Due to the importance of these water resources, it is critical that we improve our understanding of recharge mechanisms for karst aquifers.

The epikarst, or the "skin" of karst aquifers (Bakalowicz, 2004), serves as the interface between surface environmental conditions and karst aquifer functioning. Deemed a "critical zone" (Mangin, 1975), the epikarst regulates water quantity, water quality, and ecosystems in karst aquifer systems. The epikarst, which is also called the subcutaneous zone, is the region of vegetation, soil, and weathered bedrock at the top of the vadose zone in karst aquifers. Due to its extreme heterogeneity, recharge and storage in the epikarst are notoriously difficult to characterize. However, much research has been conducted to characterize epikarst controls on recharge to karst aquifers (e.g., Bakolowicz, 2004; Baldini et al., 2006; Ford and Williams, 2007; Klimchouk, 2004; Padilla et al., 1998; Smart and Friederich, 1987; Tooth and Fairchild, 2003; Vesper et al., 2000; White, 2002). Results of these studies have shown that not only does the epikarst determine how much, how fast, and at what time of year rainwater recharges an underlying karst aquifer, but is also linked with if, how, where, and when contaminants are transported from the surface to the aquifer.

1.1 Epikarst Formation

Epikarst forms near the surface due to enhanced dissolution of limestone and/or dolomite from dissolved CO_2. CO_2 enrichment occurs in soils via microbial respiration. Together, these processes create carbonic acid, which lowers the pH of infiltrating waters and enhances calcite

and/or dolomite dissolution. This process can be reversed with depth, however, because as infiltrating waters move from the epikarst into open conduits, pCO_2 degasses, causing calcite precipitation and speleothem formation (Ford and Williams, 2007). In addition to chemical dissolution, epikarst formation relies heavily on the effects of physical unloading from weathering and stress release to produce fractures and joints, along which enhanced dissolution may propagate (Klimchouk, 2004). It is important to note that epikarst is not always present, but in a well-developed karst aquifer, the epikarst is typically 3 to 10 m thick (Williams, 2008).

1.2 Epikarst Structure

Although the form and function of the epikarst are highly variable due to differences in lithology, structural setting, geomorphology, and climate, there are some common characteristics of epikarst that can be generalized. Due to its proximity to the surface, the epikarst is subjected to enhanced chemical and physical weathering, which results in a zone of higher hydraulic conductivity that diminishes with depth (Figure 1) (Ford and Williams, 2007). This permeability contrast between the epikarst and the underlying bedrock can result in a perched aquifer within the vadose zone. As a consequence, water is temporarily stored at the base of the epikarst via capillary forces and ponding in dissolution pockets (Ford and Williams, 2007). Below the epikarst, hydraulic conductivity is much lower, except where integrated flow networks have converged to more hydraulically conductive conduits (i.e. cave passages) and fractures where fast (turbulent) flow dominates (Klimchouk, 2004).

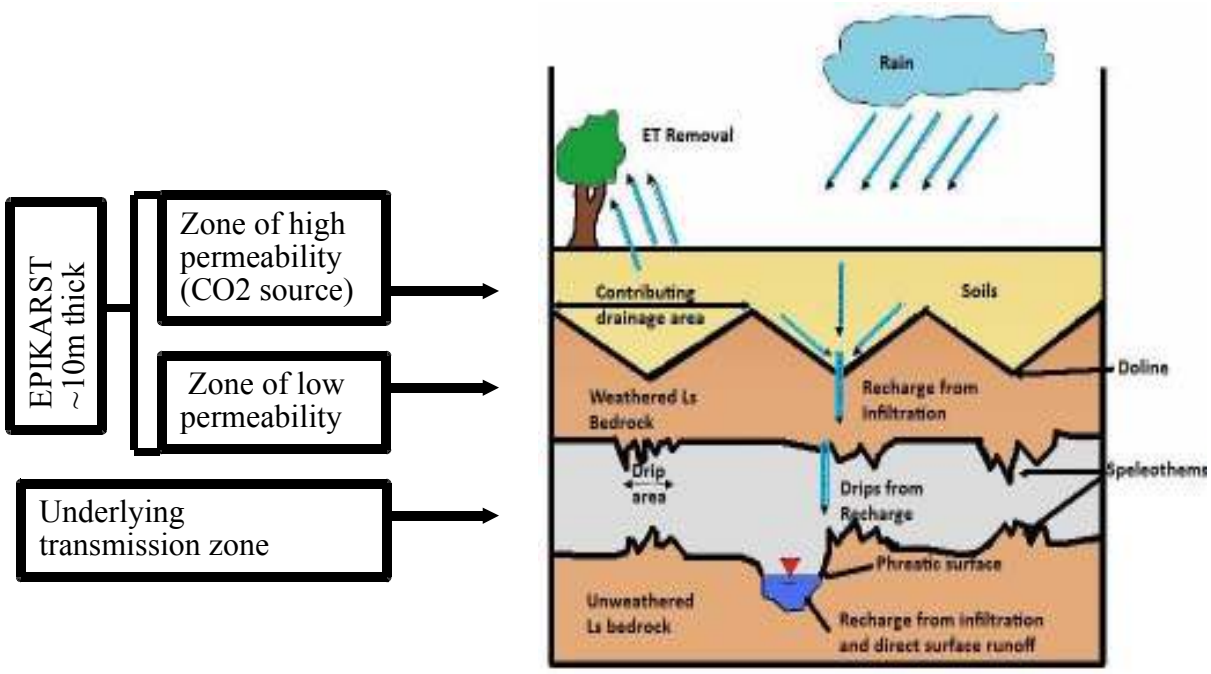

Figure 1. Idealized cross-section of epikarst showing permeability contrast with depth.

1.3 Epikarst Hydrology

In recent years, several studies have improved characterization of flow in the epikarst. Using Mangin's (1975) hydrograph recession analysis, Padilla et al. (1994) was able to use drip hydrographs to differentiate flow from the epikarst as baseflow or quickflow, where baseflow (or diffuse flow) represents seasonal flow from the perched saturated zone through small fissures and matrix porosity, and quick flow represents flooding in conduits caused by storm events.

Mangin's early hydrograph work also helped to develop the concept of "flow-routing" or the notion that different flow paths exist (i.e. from high to low porosity and permeability: conduits, fractures/fissures, and matrix porosity) that activate in a hierarchical succession based on the amount and timing of recharge. By plotting semi-log discharge over time, linear segments are interpreted to represent flow contribution from different flow paths (Ford and Williams, 2007). Quickflow, represented by a steep slope near the peak discharge, is likely found in higher conductivity compartments that are quickly drained. Baseflow, represented by a gradual slope near the base of the hydrograph curve, indicates long-term storage and diffuse flow through matrix porosity. Slope reduction indicates removal of a dominant flow path.

Smart and Freiderich (1987) further defined the varied types of flows within the epikarst based on the discharge and discharge variability (coefficient of variation). Their defined types include seepage flow (low discharge, low variability), vadose flow and shaft flow (higher discharge, higher variability), and subcutaneous flow (variable discharge, high variability). This hydrologic characterization has been improved through use of geochemical data, including dissolved organic carbon (DOC) (Baker et al., 1997), major cations (Fairchild et al. 2006; Baldini et al., 2006), and electrical conductivity (Genty and Deflandre, 1998). Results of these studies have been used to improve characterization of speleothem growth, which is used for paleoclimate analysis.

Results from the above studies on epikarst flow show that high heterogeneity and scaling issues (e.g., local, regional, global) make it difficult to generalize epikarst's control on aquifer recharge. However, the need to understand these high yield water resources is paramount for managing increasing demands. The objective of this project was to develop a comprehensive model of epikarst hydrodynamics as water progresses through the epikarst using intensive field techniques. To accomplish this objective, long-term (up to three years) continuous hydrology measurements from precipitation, soil moisture, speleothem drips, and an underground stream in James Cave in Pulaski County, VA, were used to 1) delineate spatial and temporal recharge patterns, 2) estimate effective recharge and quantify the size of the contributing drainage area to drips, 3) characterize the number and permeability of flow paths contributing to drips, 4) to characterize storage capacity in the epikarst. Results are used to create a conceptual model of the epikarst that underscores how field scale variations play an important role in epikarst's regulatory control on storage and water quality.

2. FIELD SITE

2.1 Location and Climate

James Cave is located in Pulaski County, Virginia (Figure 2) at approximately 600 m above sea level. The field site is located in an agricultural setting that is used for cattle production (Figure 3). Prior to 2008, fertilizer was applied for hay production. NPK fertilizer is still used in adjacent fields, upgradient from the monitoring site.

Figure 2. Pulaski County, VA.

Figure 3. James Cave sinkhole entrance

The field area at James Cave is located in a temperate climate zone, and experiences equally long winters as summers. According to a weather station in Radford, VA (Southeast Regional Climate Center, 2010), the area is subject to an average annual temperature of 11.3 °C and average annual precipitation of 92.4 cm (Period of record: 1969-2009).

2.2 Geology and Soils

James Cave formed within limestones and dolostones of the Cambro-Ordovician Elbrook and Conococheague formations within the Valley and Ridge physiographic province. Bedrock fracturing/jointing developed primarily as a result of the Pulaski fault system, a complex series of ENE trending Alleghanian age thrusts (Bartholomew, 1987). Subsequent karstification created pathways for percolation via enhanced dissolution along fractures and joints. The soils overlying James Cave, as defined by the USDA, are composed of both the Lowell silt loam and the Wurno-Newbern-Faywood silt loam (USDA-NRCS, 2006). Both soils are derived from residuum weathered from limestone and shale, range in thickness from 0.25-2 m between ground surface and bedrock, have a low to moderate water capacity, and have a slow infiltration/transmission rate when thoroughly wet. The soils contain up to 3% organic matter, have a pH range from 4.5-7.8, and have an effective cation exchange capacity of 4-17 meq/100g (USDA-NRCS, 2006).

2.3 Hydrology

James Cave is located in a large, low-relief karst plain that is internally drained and recharged, and it is hydrogeologically representative of much of the Shenandoah Valley, a sub-province of the Appalachian Great Valley. The Great Valley is the largest contiguous karst region in the Appalachians, extending from Alabama to New York, and as such, is a regionally important carbonate aquifer (Trapp and Horn, 1997). At James Cave, karstic limestone and dolostone aquifers contain underground streams that discharge at springs along the New River. Field observations indicate that overland run-off into the entrance sinkhole can occur, but only following intense precipitation events.

Attempts to determine the source and discharge point of the stream in James Cave via dye tracing were unsuccessful. Based on the lateral extent of limestone around the field site, it is assumed that the stream is derived from autogenic sources (i.e. epikarst recharge via diffuse infiltration from precipitation deposited directly onto a carbonate landscape) and not allogenic sources (i.e. recharge derived from flows off of non-carbonate regions).

3. CAVE INSTRUMENTATION AND SAMPLING METHODS

3.1 Sampling Sites

One surface station, three soil lysimeters, three epikarst drip stations, and one stream station were instrumented in 2007-2008 to collect long-term hydrologic and geochemical data at James Cave (Table 1). Additional surface climate data not measured at the study site were obtained from the Virginia Tech Kentland Farm (Virginia Agricultural Experiment Station, 2010), which is located 4 miles from James Cave.

3.2 Cave and Epikarst Structure

A topographical survey (Figure 4) of the cave was performed and tied into surface elevation to determine the relative orientation of the epikarst drip monitoring stations (MS1-3) and to determine the thickness of the epikarst overlying the stations (elevation data is for NAVD88 computed using Geoid03). Based on the survey, MS1 and MS2 are ~15 m apart, ~50 m west of cave entrance. MS3 is ~60 m east of the cave entrance. The sites are located far enough

from the cave entrance to minimize the influence of surface environmental conditions. Depth of the monitoring stations below ground surface are 8 m (597 m AMSL) at MS1 , 10.7 m (595.1 m AMSL) at MS2, and 7 m (593 m AMSL) at MS3.

Electrical Resistivity Tomography (ERT) surveys, using a dipole-dipole array with 1 m spacing, were centered over each drip station and oriented approximately perpendicular to the cave length to make inferences about epikarst structure (Figure 5). An AGI Super Sting electrical resistivity unit with a 64 electrode cable was used to measure the profiles. In Figure 6, low resistivity areas are shown in blue and are interpreted to represent moist soils and highly weathered bedrock. The high resistivity areas shown in red and yellow are interpreted to represent voids or dense bedrock. ERT allowed for identification of drip and soil monitoring stations relative to zones of varying resistivity within the epikarst structure.

Table 1. Discharge Instrumentation by Monitoring Station

Monitoring horizon	Station name and depth (elevation)	Climate data	Precipitation or discharge measurement (per 10 minutes)
Surface	Precipitation: ~1 m above ground surface (~605m AMSL)	Air temperature, relative humidity (additional climate data collected from Kentland Farm)	Tipping bucket rain gauge
Epikarst drips 3 stations	MS1: 8 m (597 m AMSL) MS2: 10.7 m (595.1 m AMSL) MS3: 7 m (593 m AMSL)	Air temperature, relative humidity	Drip collection tarp to tipping bucket rain gauge
Cave stream	Stream: ~12 m	Air temperature, relative humidity	V-notch weir

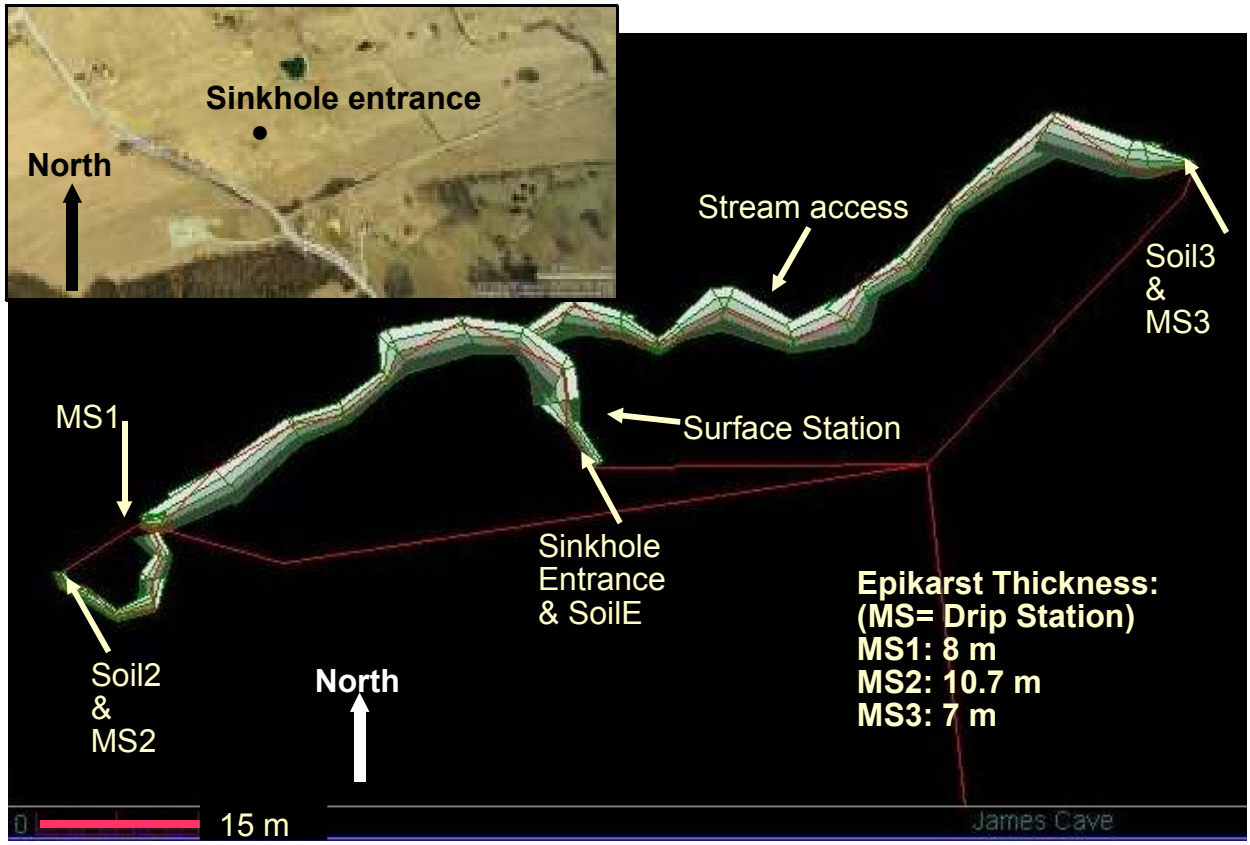

Figure 4. Aerial view of site survey (survey produced courtesy of Tom Malabad) showing cave passages and station orientation relative to sinkhole entrance.

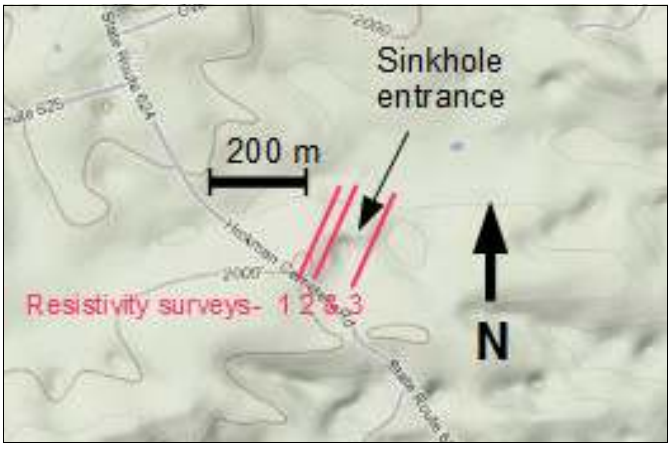

Figure 5. Approximate orientation and location of ERT survey lines. Note terrain view shows several sinkholes within the map view.

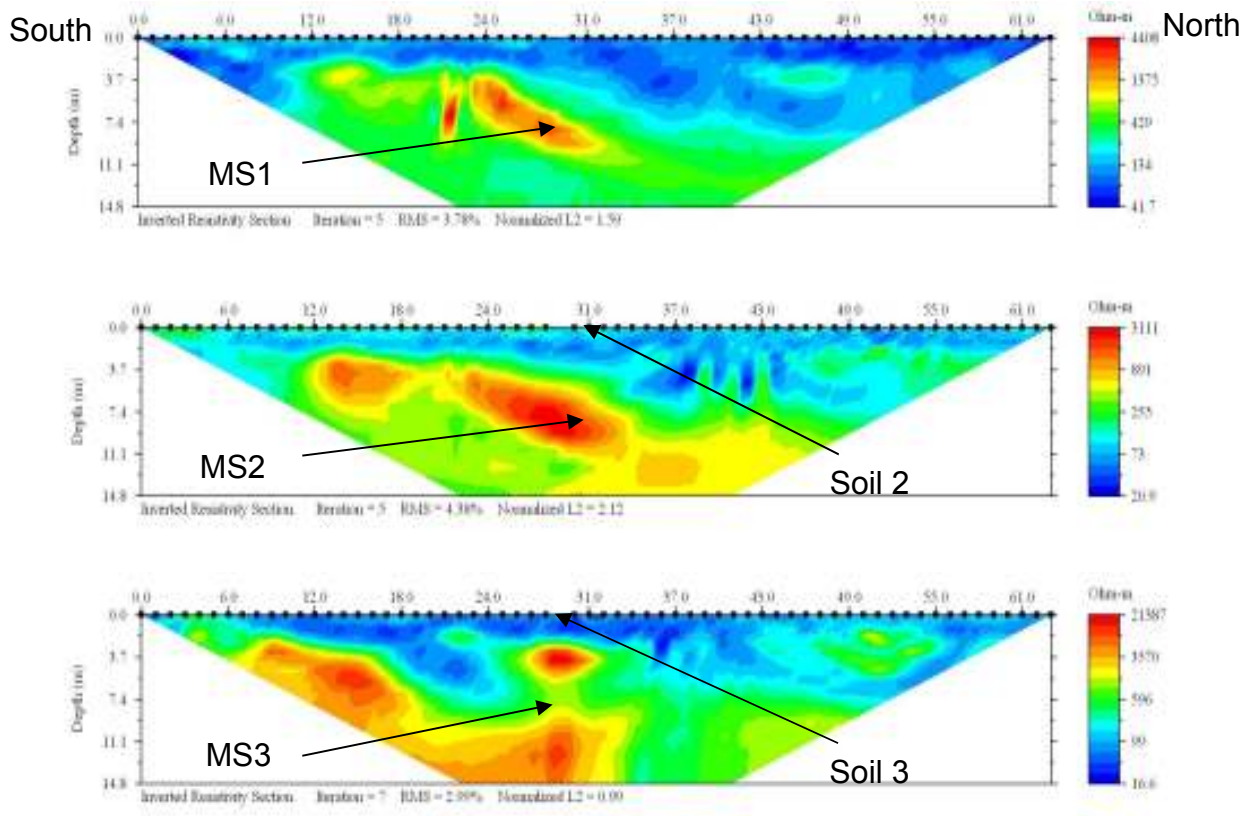

Figure 6. ERT survey to visualize epikarst structure and relative station orientation.

3.3 Instrumentation Details

The surface precipitation station (Figure 7) was instrumented with a tipping bucket rain gauge to measure rainfall, and it also measures air temperature and relative humidity (Table 1). Three tension lysimeters (Figure 8) are located approximately 1 meter below the ground surface and are used to collect grab samples of soil moisture. Three speleothem drip stations are instrumented with a collection tarp and tipping bucket system to measure drip rates (Table 1). Custom-built suspended tarps (Figures 9 & 10) collect and funnel drip-water from areas with active speleothems through a biological strainer and into a tipping-bucket rain gauge (Figure 11). Stream discharge is measured using a V-notch weir, pressure transducer, and barometric logger (Table 1). Discharge measurements are recorded continuously, every 10 minutes. Monitoring stations also collect geochemical and biological samples, however, these are not discussed in this thesis.

Figure 7. Surface station

Figure 8. Lysimeter prior to installation

Figure 9. MS1 drip tarp & flow cell

Figure 10. Data download at MS3

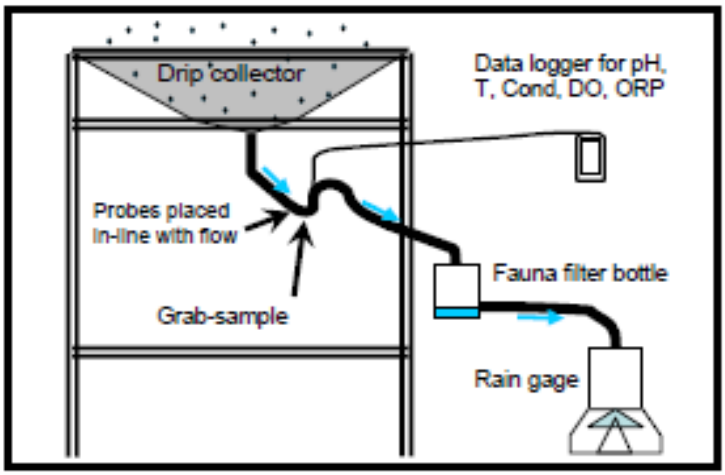

Figure 11. Schematic showing drip sampling setup. The setup of the geochemical sonde with datalogger and collection of biological samples are not described in this thesis.

4. DATA ANALYSIS METHODS

4.1 Potential Evapotranspiration Estimation

Potential Evapotranspiration (PET) is a modeled estimate of the environmental demand for water, assuming ample water is available. Surface climate data (i.e. daily Max./Min. temperature, average wind speed, global solar radiation, and daily Max./Min. relative humidity) obtained from the Virginia Tech Kentland Farms site, were used to estimate daily PET with the Penman-Monteith method (ASCE-EWRI, 2004). A spreadsheet model (PMday) written by Snyder and Eching (2007, 2009) was used to perform PET calculations. Details of the ASCE Penman-Monteith model and how PET is calculated can be found in the references cited above.

4.2 Effective Recharge and Contributing Drainage Area Estimation

Effective recharge (ER), also called precipitation excess, is the proportion of total precipitation received that is not removed by evapotranspiration. ER can be estimated according to the following water balance equation:

$$ER = Precipitation - PET \quad (1)$$

where Precipitation and PET are calculated daily and then summed over a specified interval (see explanation below). The underlying assumptions for use of this equation are that 1) runoff is negligible compared to infiltration, 2) when PET > Precipitation, then ER = 0 so that soil moisture isn't a limiting parameter (i.e. soil moisture may be present but there isn't enough for infiltration and recharge to occur), and 3) there is complete hydrologic turnover (i.e. change in storage is zero) in the unsaturated zone on a yearly scale (i.e. October to following October). It is important to note that PET estimates can be significantly higher than AET during the summer when soil moisture is low. To determine the appropriate time interval over which ER should be calculated using Equation (1), the sum of the calculated ER over a specified time interval (e.g. day, week, month, season, year) was compared to the sum of the measured drips over that same time interval to find the visual best fit between the two data signals.

By optimizing the fit between drips and ER, we assume that PET approaches AET because based on the assumption that ER = 0 when PET > Precipitation, then we can expect that compilation periods with too short an interval will underestimate PET, and periods compiled with too long an interval will overestimate PET. By identifying an interval that allows for the best fit between drips and effective recharge, we can determine the most appropriate effective recharge rate. Plots over different intervals showed that a monthly time interval provided the best match between calculated ER and observed drips. This choice is supported by other studies on effective recharge, which have also used a monthly interval (e.g., Genty and Delfandre, 1998; Baldini et al., 2006). Despite a close match between ER and drips on a monthly basis, it is likely that this method still provides a slight overestimate of ER, and thus it is recommended that antecedent moisture conditions also be quantified in future research to better characterize PET.

Using the monthly time interval, ER was then calculated for each recharge season (i.e. 10/07 to 10/08 and 10/08 to 10/09). Next, by dividing the total seasonal volume of measured drips (m^3) by the total seasonal ER (m), the contributing drainage area (CA), or recharge area, was calculated to each drip site for each recharge season. Based on gaps in the data record, CAs were not calculated for MS1 and MS2 during the recharge season from 10/08 to 10/09. Although MS3 is missing some data from 10/07 until 1/08, it was possible to calculate CA for MS3 from 10/07 to 10/08 by assuming that the site received no drips until February 2008. This assumption is supported by precipitation and drip data from other stations that suggest no recharge occurred

during this period.

4.3 Hydrograph Recession Analysis

Hydrographs from the drip and stream sites were analyzed using recession analysis to characterize lag time, the number and permeability of flow paths, and maximum storage capacity based on the methods of Mangin (1975) and Padilla et al (1994). According to Ford and Williams (2007), Maillet (1905) first described karst spring hydrograph recession using the following exponential expression:

$$Q_t = Q_o * e^{(-\alpha * t)} \quad (2)$$

where Q_t is the discharge (m^3/s) at time t, Q_o is the initial discharge at time zero, t is the time elapsed between Q_t and Q_o, and α (t^{-1}) is the recession coefficient. Equation 2 is based on a linear relationship between hydraulic head and flow rate during baseflow conditions, and the curve of the recession can be represented as a straight line with a slope of (-) α on a semi-log plot. The recession coefficient can be expressed as (Ford and Williams, 2007):

$$\alpha\ (slope) = (logQ_1 - logQ_2)/(0.4343*(t_2 - t_1)) \quad (3)$$

where Q_1 and Q_2 are discharges that correspond with different times (t_1 and t_2) for a discharge event.

4.4 Dynamic Volume Calculation

The dynamic volume is the volume of water stored in the saturated zone above the level of some outflow point, and it can be estimated using hydrograph data. It is possible to model flow through karst according to the following expression (Padilla et al., 1994):

$$Q_o = (Q_b * e^{(-\alpha * t)}) + ((q_o * (1 - nt))/(1 + \varepsilon t)) \quad (4)$$

where n characterizes the mean velocity of infiltration (close to 1 when fast infiltration is dominant) and can be determined by taking the reciprocal of t = 0 (i.e. $1/t_i$). q_O is the difference between the total outflow, Q_O, at the spring at t = 0 and a baseflow component termed Q_b. The function is defined between t = 0 and t = 1/n, which is the duration of the flood recession. The

coefficient $\mathcal{E}$ characterizes the importance of the concavity of the quickflow recession curve in terms of t^{-1} and is small (<0.01) when infiltration is very slow.

By integrating the baseflow component, it is possible to determine the dynamic volume, $V_{b,}$ contributed from baseflow reserves (Padilla et al., 1994):

$$V_b = c * Q_b / \alpha \tag{5}$$

where c is a constant (i.e. When Q_b is in m^3/s and α is in days, then c=86,400). In a complex recession that consists of many recession coefficients, the dynamic volume is the sum of the component values.

Floodwater volume (V_f) at half of the peak discharge, or $t_{0.5}$, is calculated by (Padilla et al., 1994):

$$V_f = q_o / \mathcal{E} * (\mathrm{Ln}\,(1+\mathcal{E}t) * (1+(n/\mathcal{E})) - nt) \tag{6}$$

where $t_{0.5}$ is the time required for the initial flow to diminish by 50%, and can be calculated from (Ford and Williams, 2007):

$$t_{0.5} = (\mathcal{E} + 2\mathrm{n})^{-1} \tag{7}$$

4.5 Master Recession Curve Separation

Using a fully automated objective-based program for master recession curve (MRC) separation (Posavec et al., 2010), it was possible to generate a MRC for each station based on averages of discharge data for the entire period of record. MRC generation allows for a more quantitative assessment of contributing flow paths and storage compartments than the graphical techniques discussed in section 4.3, and can be used to make predictions about flow and storage characteristics in the epikarst over each drip station. Details of the MRC separation method and program can be found in Posavec et al. (2010).

5. RESULTS AND DISCUSSION

5.1 Recharge

5.1.1 Spatial and Temporal Recharge Patterns

Figure 12 shows drip and stream discharge response to cumulative precipitation for an 800 day period of record (September 2007 to December 2009). There is a marked difference in precipitation and resulting drips between 2008 and 2009, allowing for a useful comparison between a dry year (2008) and a wet year (2009). All subsurface stations show responses to precipitation events, indicating a hydraulic connection to the surface. Calculation of lag times, or the difference in time between peak precipitation rate and peak drip rate, indicate that after significant seasonal recharge, drips occur two to five hours after initiation of a rain event. During the growing season, however, precipitation often does not trigger drips because most, if not all, infiltrating water is removed by evapotranspiration. Drips are re-initiated only after there has been enough precipitation to reactivate hydraulic pathways in the epikarst, a process that can take up to several months (Figure 12). Variations in lag time throughout the recharge season show that sustained recharge results in progressively shorter lag times between rain events and drip events. As permeability in the unsaturated epikarstic zone depends on moisture content and pressure head, we can expect that lower moisture content results in lower permeability. Another interesting pattern to note is that short duration precipitation events trigger relatively long drip events, suggesting flow diffusion and complex flow routing in the epikarst.

Following Smart and Friederich's (1987) epikarst flow type classification system, discharge data were used to assess the type of flow inlet to each drip station based on a semi-log plot (Figure 13) of the maximum discharge vs. the coefficient of variation. Results show that all three drip monitoring stations plot within the field of “seasonal drips”. According to Smart and Friederich (1987), stations that plot within the seasonal drip field show an increase in total unsaturated zone storage with depth, and it is implied that these drips sustain baseflow to deeper inlets (e.g., cave stream). Other drip studies that have used this classification system have a wider variety of types (seepage, seasonal, vadose, subcutaneous) represented in their drips (e.g. Baker et al., 1997; Baldini et al., 2006 Fairchild et al., 2006), but these studies have measured

individual stalactites, while in this study, the use of the drip tarp integrates multiple drips, and thus homogenizes the hydrologic characteristics of individual drips.

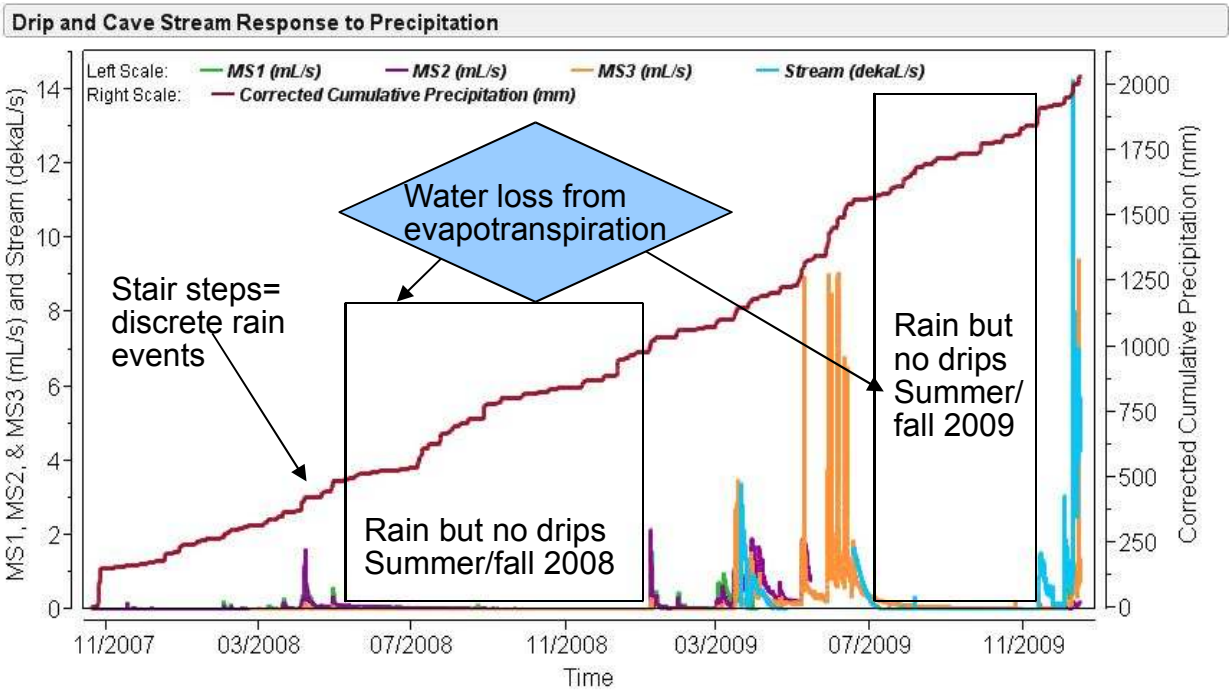

Figure 12. Drip and stream response to precipitation (September 2007 to December 2009).

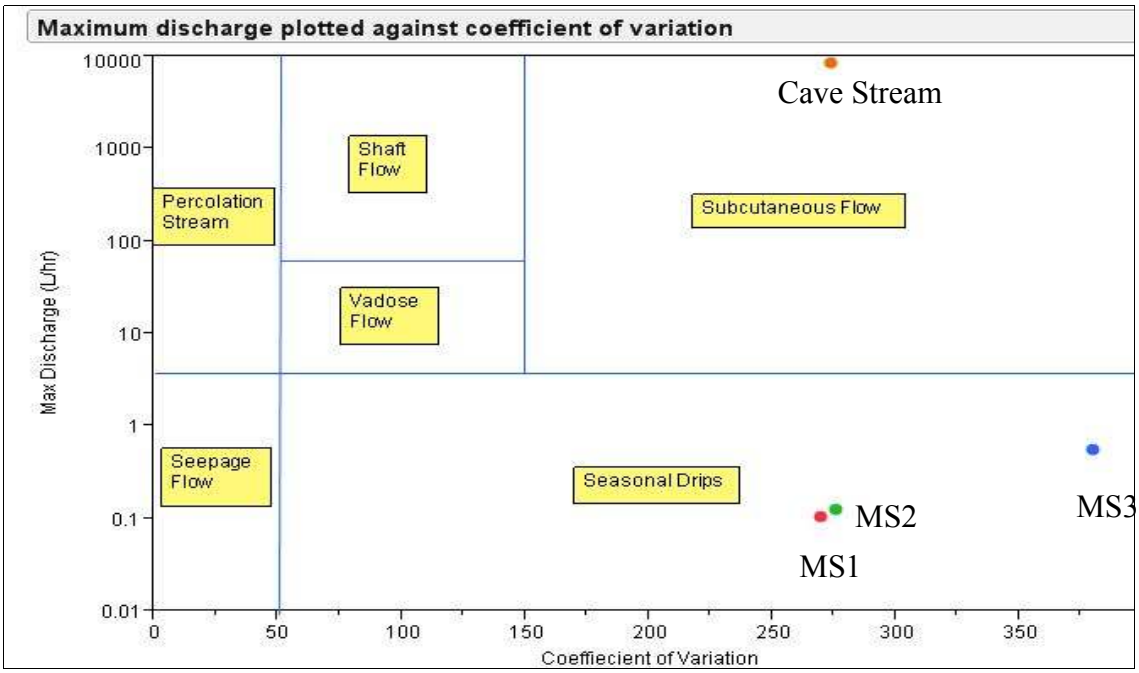

*Figure 13. Maximum measured discharge plotted against coefficient of variation (standard deviation/mean*100). Fields denoted were originally defined by Smart and Friederich (1987).*

5.1.2 Effective Recharge and Contributing Drainage Areas

Using equation 1, effective recharge (ER) was calculated with measured daily precipitation data and calculated daily PET data. ER rates were estimated by compiling data for several different time intervals. Figure 14 only shows the results of ER compiled on a monthly basis because that was found to be the best fit to our drip data. During the recharge season from 10/07 to 10/08, ER was estimated to be 23%, and during the recharge season from 10/08 to 10/09, ER was estimated to be 34% of total precipitation received during that season. These values correspond well with 28% annual ER as predicted for the region with Thornthwaite's Method by the University of Virginia Climatology Office (2010). It also corresponds with another measurement of ER (30%) through mantled sinkholes from the nearby Kentland Farms site (Schwartz and Schreiber, 2009).

Next, the contributing drainage areas (CA) for the drip stations were estimated for each recharge season. Note that no drip data were available at MS1 from 4/09 to 7/09 and at MS2 from 5/09 to 9/09 due to equipment malfunction. Although Figure 14 shows no drips during these periods, based on precipitation and comparison with MS3 drip data, it is likely that these sites received considerable recharge. After accounting for all data gaps and assuming 23% ER from 10/07 to 10/08 and 34% ER from 10/08 to 10/09, it was possible to calculate CAs based on available drip and precipitation data for these periods. This was performed by dividing the total annual volume of measured drips (m^3) by the total annual ER (m) for each period. Table 2 includes the results of the CA calculations.

It is interesting to note that the CA varies by site and by year, suggesting the importance of seasonal climatic variations and differences in storativity between sites. By comparing CAs between sites for the period from 10/07 to 10/08, we see that MS3 receives flow from a much smaller area than other drip stations. By comparing MS3 during the 2008 and 2009 recharge seasons, we see that increased recharge in 2009 increases the overall size of the CA to MS3.

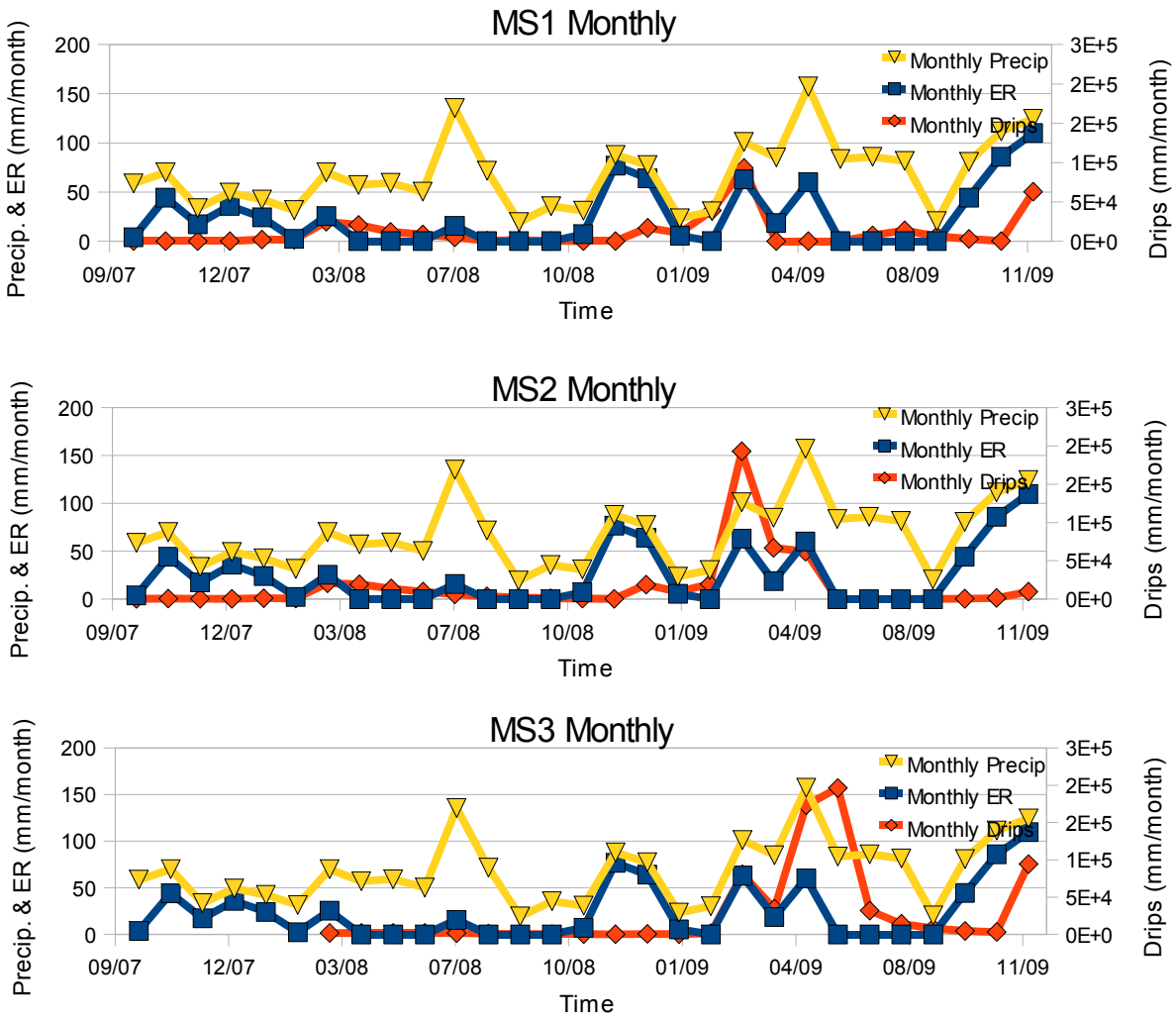

Figure 14. Comparison of precipitation, calculated effective recharge, and drip data for MS1, MS2 and MS3. Data compiled on a monthly basis to provide best fit between ER and Drips.

Recharge Season	CA to MS1 (m^2)	CA to MS2 (m^2)	CA to MS3 (m^2)
10/07 to 10/08	6.33	6.52	1.02
10/08 to 10/09	NA	NA	24.97

Table 2. Calculated contributing drainage areas for each drip station. Assumes 23% ER for 10/07 to 10/08 and 34% ER for 10/08 to 10/09.

5.2 Permeability and Flow Restrictions

5.2.1 Slope of Hydrograph Recession Curves

Hydrographs reveal important information about the flow and storage characteristics contributing to flow at a monitoring station. By comparing multiple hydrograph recessions for one station (e.g. MS3 in Figure 15), it is clear that many recessions take on similar shapes across many drip events of varying magnitudes. This suggests that the shape of the hydrograph is controlled in part by the amount of discharge received, but also by variations in the number and permeability of flow paths that actively contribute to drips at varying levels of discharge (Ford and Williams, 2007). Semi-logarithmic plots of drip discharge vs. time reveal linear and non-linear segments along the recession that can be interpreted to represent transmission in different flow paths of varying permeability. Although it is likely that these flow paths are not isolated from one another and that mixing persists to some degree, we assume that as flow recedes, a segment transition along the recession curve signifies a change in the number and type (i.e. high or low porosity) of transmissive pathways contributing to the drip station. Another assumption is that steep slopes indicate discharge from higher permeability compartments, moderate slopes indicate mixing between high, medium, and low permeability compartments, and long and shallow slopes represent discharge from long-term storage in low permeability compartments.

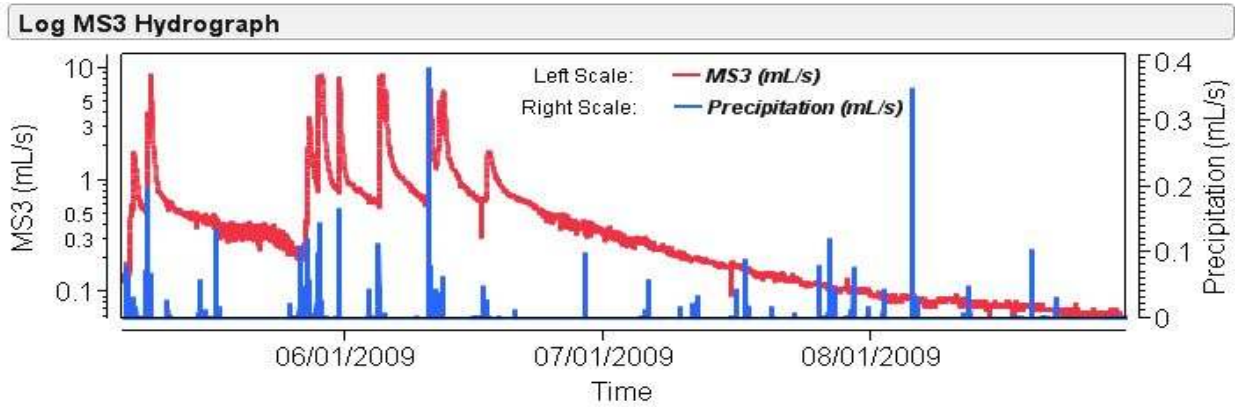

Figure 15. MS3 hydrographs showing similar shaped recessions across several recharge events.

Using equation 3, recession coefficients (α) were calculated for linear segments along multiple hydrograph recession curves for each drip station. It is assumed that each change in α signifies a transition in the dominant flow path contributing to flow. Recession curves chosen for analysis were those that had a long period of recession in order to avoid distortion by subsequent rain events. Figure 16 shows a single hydrograph recession for MS3 that has been isolated to show trend lines and their corresponding recession coefficients. From the angle (steep to shallow) and relative length of the segments, it can be inferred that as the recession curve recedes, the dominant flow paths change from fast flow through well-drained fractures and conduits ($\alpha 6$ & $\alpha 5$), to moderate flow through fissure networks ($\alpha 4$ & $\alpha 3$), and finally to slow/diffuse flow through residuum and soils ($\alpha 2$ & $\alpha 1$).

Table 3 includes a summary of the recession coefficients from each drip station based on an average of the results for like segments (i.e. segments with similar slopes and lengths). It is important to note that smaller rain events may not always activate higher level recession coefficients. By comparing recession coefficients between sites, we see that MS3 offers more pathways (i.e. six segments) to support high flow than MS1 and MS2 (i.e. five segments). This suggests that a high volume flow path contributes to drips at MS3, but the steepness and short duration of the segment indicate that the flow path must have very high permeability and offers little storativity. By comparing recession coefficients between segments, we see that low permeability in $\alpha 1$ & $\alpha 2$ offers the greatest retention in baseflow reserves. Little knowledge of mixing between flow paths and errors in graphical identification of linear segments mean that α's should be interpreted with caution when characterizing flow paths.

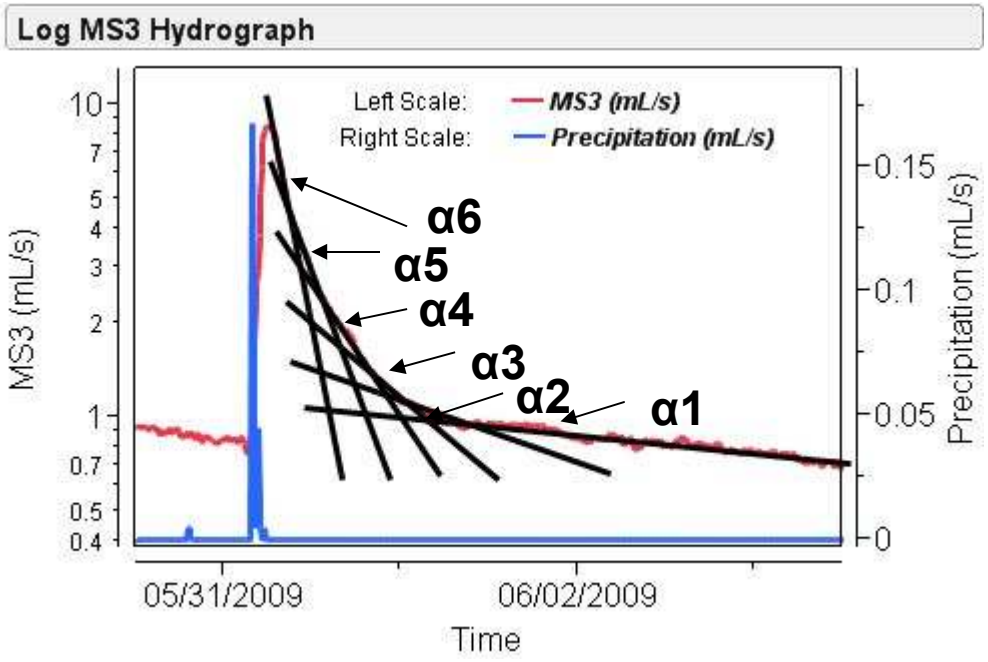

Figure 16. Example MS3 hydrograph recession showing linear segments analyzed to calculate α. For this example, five linear segments (and corresponding values of α) were identified.

Table 3. Recession coefficients per station				
α	MS1	MS2	MS3	Stream
6	--	--	6.88	--
5	1.03	2.02	3.29	--
4	0.35	0.80	1.71	1.32
3	0.11	0.40	0.49	0.22
2	0.08	0.19	0.15	--
1	0.04	0.06	0.05	--

Table 3. Average recession coefficients from each drip station based on an analysis of like segments (i.e. segments with similar slope and length) from each station. Events analyzed: MS1& 3= five events, MS2=six events, Stream= two events. Linear segments based on visual best fit.

Previous researchers have typically identified two to three segments in karst spring hydrograph recessions (Ford and Williams, 2007). For instance, at Ombla springs in Croatia, Milanovic (1976) regularly identified three segments, which he interpreted to reflect porosity decreases in the dominant flow paths from fractures and conduits to fissures, and then to matrix porosity. Our results, which typically contain four to six segments, likely result from the subjective nature of the segment identification, which may result in an overestimate of the

number of contributing flow paths. By looking at the magnitude of recession coefficients in Table 3 we see that some coefficients (e.g., $\alpha 5/\alpha 4$ and $\alpha 2/\alpha 1$) may actually overlap, and as expected, recognition of the true recession coefficient is confounded by mixing between different permeability flow paths.

For a more objective assessment of flow components, master recession curves (MRCs) were generated for each drip station that allow for identification of average aquifer parameters based on discharge data from the entire period of record. Information from MRCs can be used to predict the most probable recession scenario at drip stations. Using a fully automated objective-based method for MRC separation (Posavec et al., 2010), it was possible to generate a MRC for each station with average recession coefficients per segment that allow for a more objective assessment of contributing flow paths and storage compartments. Figure 17 shows an example MRC for MS3.

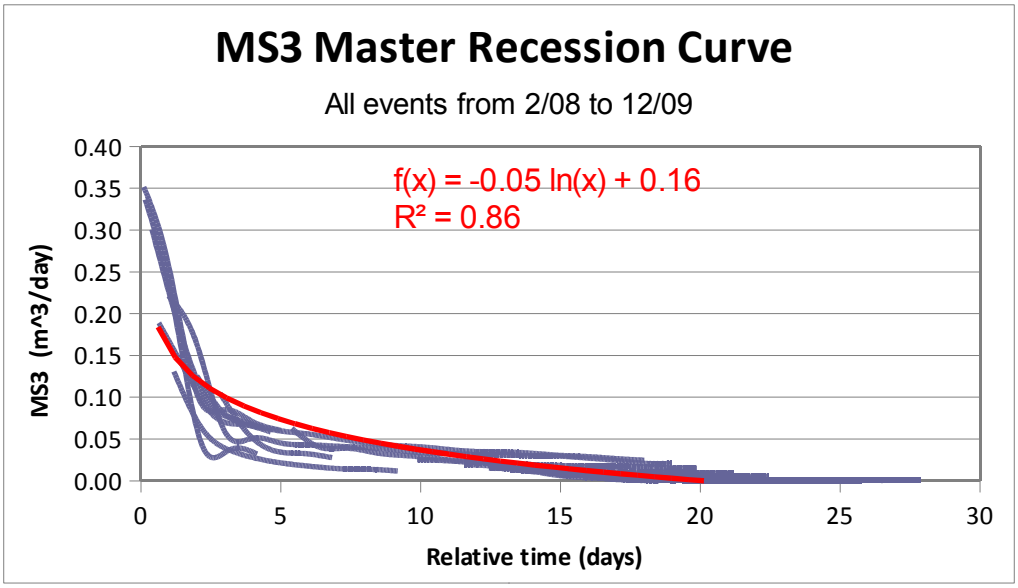

Figure 17. Example Master Recession Curve from MS3 for all events from 2/08 to 12/09. Gray lines are based on actual recession data from entire period of record, and red content is the MRC, or best fit expression to all of the gray lines.

The MRC program (Posavec et al., 2010) selects the best fit expression (e.g., linear, exponential, polynomial, logarithmic, etc.) to the data. Results from the MRC program show that discharge from MS1 and MS2 is best represented by a polynomial expression, and that discharge from MS3 is best represented by a logarithmic expression. This difference could be

related to differences in flow restrictions and flat peak discharges at MS1 and MS2, which are not observed at MS3. It is important to note that recession coefficients for individual segments are only calculated using an exponential expression, regardless of the best fit identified for the overall MRC.

Table 4 includes recession coefficients determined from the MRC separation program. From this, we see fewer segments identified in the hydrograph recessions, as compared to those identified using the visual method (Table 3). This could be explained by limitations of the MRC program as it can generate a maximum of three segments, or it may suggest that the visual graphical method of recession coefficient analysis provides an over-estimate of the number of linear segments because it doesn't properly account for mixing between flowpaths. It is interesting to note that the MRC program identifies three segments for MS1 and MS2 , but only two for MS3.

α	MS1	MS2	MS3
3	0.46	0.36	NA
2	0.17	0.15	0.42
1	0.06	0.19	0.3

Table 4. Recession coefficients by permeability segment determined from MRC separation at each drip station. Due to program limitations, MRC segments can only be explained by exponential functions, which provides poor fit for characterization of flat peak discharges and linear baseflow components. No α3 for MS3 because too few peak discharge data points.

5.2.2 Peak Discharge Comparisons

Comparison of hydrograph recessions in Figures 18 show that although each station has a similar response to precipitation, that there are heterogeneities in storage characteristics between stations based on differences in the shape and lag time of drip hydrographs. In 2008, when drip rates were low, hydrographs from all James Cave drip stations were similarly shaped (i.e. sharp tipped peaks with long tails). However, in 2009, after the field site received significant recharge, hydrographs began to reveal flow restrictions. Figure 19 shows that although MS2 normally receives more flow than MS3 during dry seasons, after significant recharge in 2009, MS3 discharge surpassed MS2. MS1 hydrographs in 2009 also reveal a similar phenomenon. The flattened/convex peaks at MS1 and MS2 suggest that the epikarst has reached maximum

discharge capacity (Brahana and Pennington, 2010). This also suggests that a high permeability flow path may activate at MS3 after significant recharge. One way to explain this is that the epikarst overlying MS3 is more developed (i.e. more weathered) than the epikarst overlying MS1 and MS2. It is interesting to note that there is a zone of relatively low resistivity situated over MS3 (See Figure 5 for ERT survey), which may represent a highly weathered zone that becomes hydraulically active during extremely wet periods.

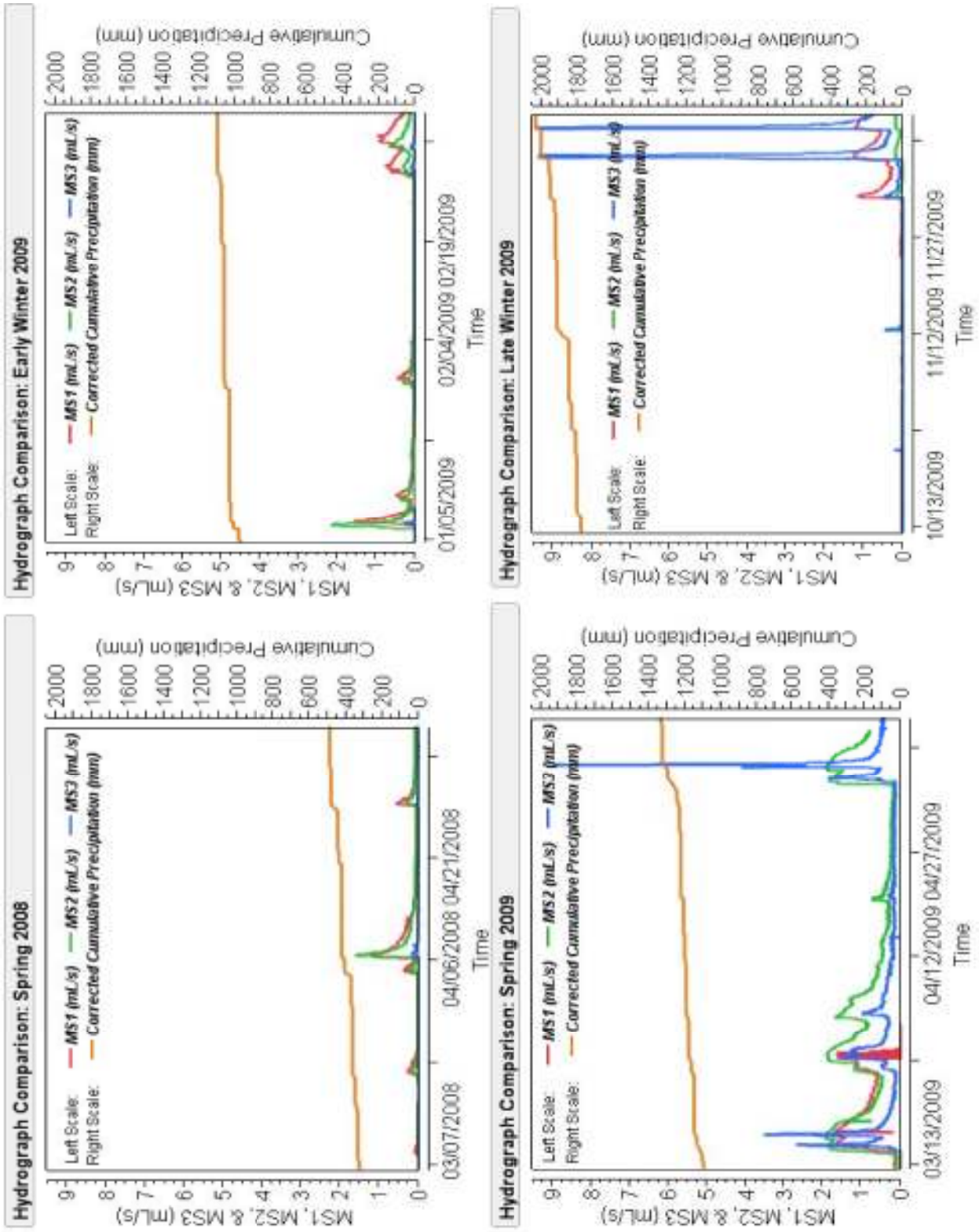

Figure 18. Seasonal recharge hydrograph comparisons.

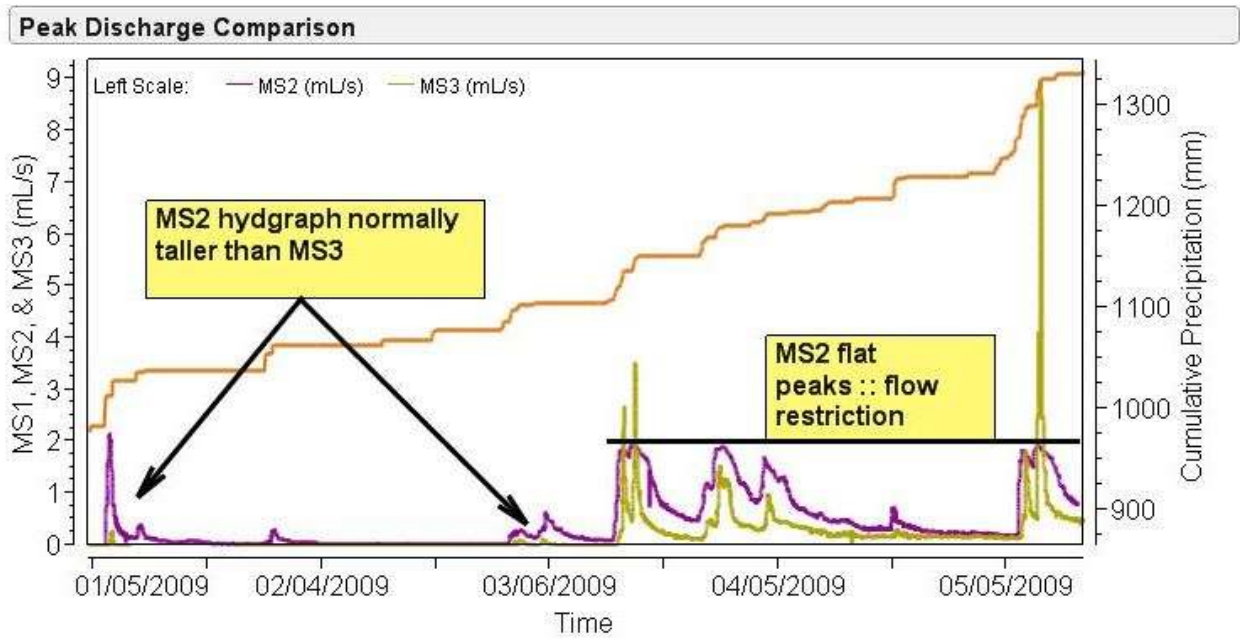

Figure 19. MS2 and MS3 peak discharge comparisons (Recall that MS1 behaves similar to MS2). Usually flow at MS2>MS3, but after significant recharge, MS2 approaches maximum capacity (reflected by the flat peaks of the hydrographs), while MS3 appears to overflow into a higher permeability pathway.

By comparing drip responses to each other between several precipitation events of varying magnitude, we see irregular patterns in which station provides the highest peak discharge for an event (Figures 18 and 19). Shifts in stations with the highest peak discharge can be attributed to karst weathering dynamics, variable antecedent moisture conditions, and the number and permeability of hydraulically active pathways that contribute to flow at varying discharges.

5.3 Storativity

5.3.1 Dynamic Baseflow and Quickflow Volumes

Hydrograph recession analysis was also used to estimate the dynamic baseflow and floodwater (quickflow) volumes for individual hydrographs. This is useful in determining if the epikarst over James Cave serves to store a significant portion of recharge as diffuse flow, or if most of the recharge that comes into the epikarst is rapidly passed through without retention. According to Mangin (1975) and Padilla et al. (1994), nonlinear segments on the hydrograph,

with steep slopes found immediately after the peak discharge, represent quickflow from storm runoff flooding larger conduits. Linear segments, with relatively low slopes, are generally much longer than the nonlinear segments, and they are located near the base of the recession curve. These long linear segments are interpreted to represent discharge from baseflow reserves held in low permeability pathways. Figure 20 shows a sample hydrograph from MS2 that differentiates between baseflow and quickflow contributions.

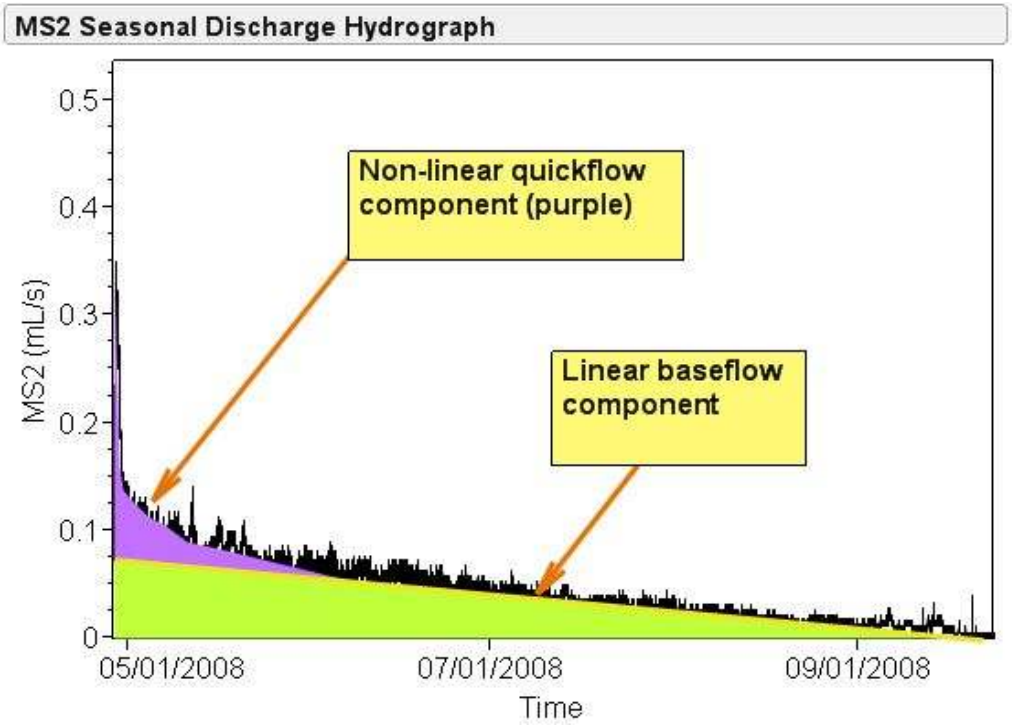

Figure 20. Example MS2 hydrograph showing baseflow (green) and quickflow (purple) discharge contributions.

By grouping the linear and nonlinear segments of a recession, parameters can be estimated that are needed for dynamic quickflow and baseflow volume calculations. To do this, hydrographs were chosen with extended recessions (i.e. ~one month) that are uninterrupted by subsequent rain events to promote easy identification of the linear baseflow segment. Next, parameters estimated from hydrographs (See Figure 21 for example) were applied to equations 5 & 6 to calculate dynamic volumes of the baseflow and quickflow components. Results of the dynamic volume calculations are summarized in Table 5.

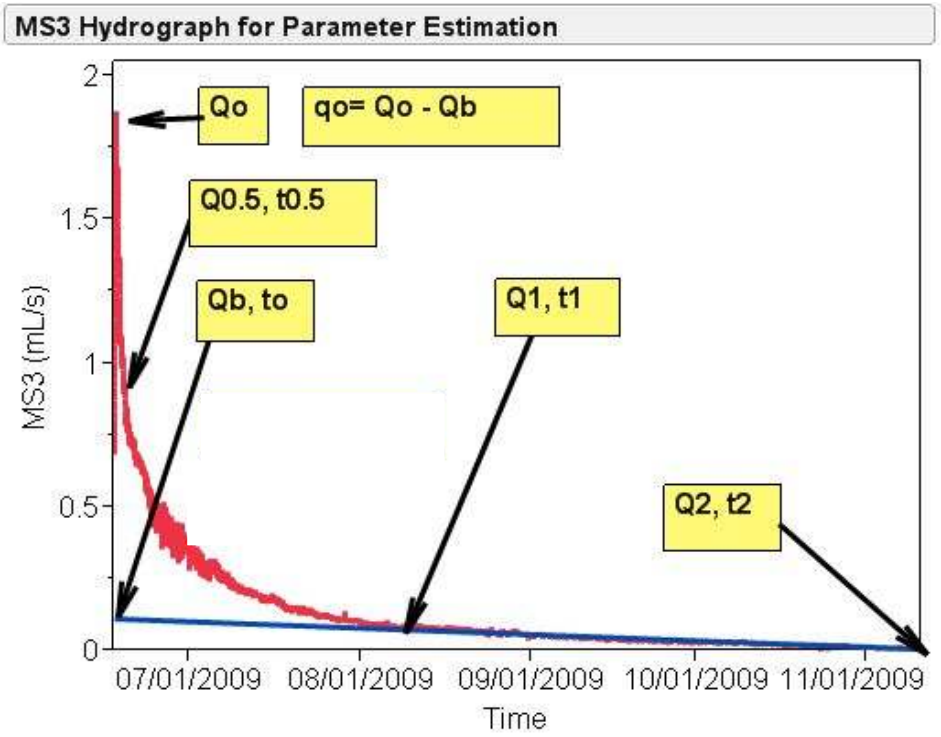

Figure 21. MS3 hydrograph (6/09 to 11/09) labeled with parameters used for dynamic volume calculation . Qo is total discharge at the beginning of the recession; Qb is discharge at the beginning of the baseflow recession; qo is discharge at the beginning of the quickflow recession; Q1, t1, Q2, and t2 are used (Equation 3) to determine recession coefficients (1/day). The area under the blue line represents storage as baseflow.

Table 3. Dynamic Baseflow and Floodwater Volume					
Station	Date	Baseflow volume (m^3)	Flood volume (m^3)	Total volume (m^3)	% Storage as Baseflow
MS1	4/6 to 4/27/08	0.160	0.204	0.364	44
MS1	4/28 to 9/21/08	0.211	0.107	0.318	66
MS2	4/6 to 4/27/08	0.267	0.162	0.429	62
MS2	4/28 to 9/21/08	0.284	0.065	0.349	81
MS3	4/6 to 4/27/08	0.023	0.012	0.036	66
MS3	4/28 to 9/21/08	0.130	0.004	0.134	97
MS3	06/17 to 11/11/09	0.390	0.629	1.019	38

Table 5. Dynamic baseflow and quickflow (flood) volume calculations at $t_{0.5}$ (half peak discharge). Percent recharge as baseflow is also shown for three different recharge events (i.e. 4/6/08, 4/28/08, and 6/17/09).

Hydrographs used in the analysis were selected because they represent recessions from seasonal recharge. In Table 5, we see that although percent storage as baseflow changes between events, discharge from the baseflow component dominates the hydrograph recessions. This

suggests that in response to seasonal recharge, the epikarst at James Cave may be able to store more than 50% of recharge as baseflow. This result corresponds with Smart and Friederich's (1987) estimate of 50% storage for GB cave at Mendip Hills, UK. Although Table 5 shows that drip stations are primarily dominated by baseflow, MS1 (event 4/6) and MS3 (event 6/17) show that a threshold exists, beyond which flow becomes dominated by quickflow. This is likely because at higher flows, more flow is directed into higher conductivity pathways. After increasing recharge, the baseflow component becomes less significant with respect to total recharge volume. Percent baseflow estimates don't account for baseflow contributions stored from preceding events.

5.3.2 Baseflow Capacity and Retention Time

MRCs provide a useful way of determining average baseflow storage capacity by separation of a representative baseflow segment based on discharge data from several hydrographs (Posavec et al., 2010). By integrating the area under the long, linear baseflow segment (Equation 5) of the MRCs for each station, it was possible to evaluate average storage capacity of baseflow reserves. In addition, by locating the point on the MRC that intersects the x-axis (time), it is possible to assess average retention time waters stored in the epikarst. Similar to the results provided by individual hydrograph analysis, MRC analysis (Table 6) suggests that baseflow reserves offer significant retention. Also, the average retention time of drip waters is about one month, which corresponds with the monthly interval used in ER calculations in section 5.1.2.

	MS1	MS2	MS3
Baseflow storage capacity (m^3)	0.2	0.24	0.42
Recession coefficient (α)	0.1	0.12	0.2
Avg. retention time (days)	29	27	23

Table 6. Average baseflow storage capacity, recession coefficients, and retention time. Results shown above are based on application of equation 5 to the baseflow component of MRCs.

5.3.3 Differences Between Stations

Despite variations in stations providing the highest peak discharges, a more regular trend was identified between stations having the largest volume stored in baseflow reserves. By comparing the areas under the long linear (i.e. baseflow component) portion of the recession curve in Figure 18, and by looking to the MRCs for retention times (Table 6), we see that MS1 has the longest retention of baseflow, followed by MS2 and MS3. This suggests that stations with the longest retention times receive flow from less efficient drainage networks that are dominated by lower permeability pathways.

By comparing the storage capacities between stations (Table 6), we see that MS3 offers the greatest capacity for storage of baseflow reserves. Comparison of 2008 and 2009 MS3 hydrographs (Figure 18) shows that higher baseflow reserves only activate after significant seasonal recharge. Additional support for a large, seasonally active storage reservoir over MS3 is supported by dynamic baseflow calculations. For instance, in Table 5, in 2008 (i.e. events 4/6/08 and 4/28/08), MS3 shows considerably lower total volume than MS1 and MS2, indicating a lower storage capacity over MS3. However, during the much wetter recharge season in 2009, we saw that discharge from MS3 surpassed MS1 and MS2 (Figure 16). Again, this provides further support for the existence of a large storage zone, high above the perched water table at MS3, which only becomes active during extremely wet seasons. Recall from Figure 12 that MS3 has a much higher coefficient of variation than MS1 and MS2, which provides additional evidence of flow path activation at higher flows. The shape of MS3 hydrographs in Figure 18 (i.e. high peaks with short tails) and the transition to a quickflow dominated system in 2009 (event 6/17/09 in Table 5) suggests that although MS3 offers significant retention of baseflow reserves, the majority of flow was derived from rapid infiltration through large permeability flow paths. This also supports the theory that inlets distributing flow to MS3 are more mature (i.e. they are more enlarged by chemical and physical weathering than MS1 and MS2).

6. CONCEPTUAL MODEL OF EPIKARST FLOW

Using a combination of the effective recharge calculations, hydrograph analysis, and calculation of dynamic volume, along with the overall spatial and temporal response of drips to precipitation events, a conceptual model of epikarst flow and storativity can be constructed based

on the following key observations.

First, effective recharge calculations show that recharge occurs seasonally (i.e. winter and early spring), and that evapotranspiration is responsible for approximately 75% water loss from total precipitation received. Seasonal recharge events increase the degree of saturation in the epikarst so that more water is stored during wetter seasons. Time lags between precipitation and drip response depend on antecedent moisture conditions. The average residence time of water stored in the epikarst is approximately one month.

Second, comparison of the contributing drainage area for each drip site (influent area: ~20 m^2) to the drip area (cave ceiling effluent area: ~3 m^2) suggests that flow paths converge with depth to produce a funneling effect. Centripetal drainage results from flow and dissolution focused along major leakage paths. Larger contributing drainage areas observed during wetter years supports the theory of preferential flowpath activation with increasing discharge. This funneling effect or convergence of flowpaths, has also been observed in outcrops (Ford and Williams, 2007) and are included in the conceptual models in other studies of the epikarst (e.g., Klimchouk, 2004).

Third, by combining survey information with trends identified from recession analysis, we can identify unique storage characteristics about each station. By ranking stations by epikarst thickness (i.e. MS2 > MS1 > MS3), precip-drip lag time (i.e. MS3 > MS1 > MS2), we see that after significant seasonal recharge, stations with a thicker and potentially less developed epikarst (i.e. less permeable) respond more quickly to individual rain events. This could mean that a thicker epikarst provides more storage potential under the premise that when the epikarst is saturated, stations with a thicker epikarst undergo a faster response due to hydraulic pressure from additional recharge. As the epikarst lies in the unsaturated zone, it is important to remember that permeability decreases as soil moisture decreases.

Fourth, by comparing average retention time of baseflow reserves (i.e. MS1 > MS2 > MS3) and contributing drainage area (i.e. MS3 > MS2 > MS1), we see that stations with larger contributing drainage areas have less efficient storativity in baseflow reserves. We assume that larger contributing drainage areas develop when the drainage structure contributing to a drip site has undergone a higher degree of chemical and physical weathering. The result is a more efficient drainage system where dissolutional enlargement of transmissive pathways has created

a less significant permeability contrast between the epikarst and the underlying transmission zone. As transmissive pathways are enlarged, porosity increases and storativity decreases to improve the internal drainage organization in the epikarst and promote quickflow. Our results correspond with previous work that attempts to characterize the "maturation" stages of epikarst development (Klimchouk, 2004). In Figure 20, the term "mature" is used to explain how in well-drained areas, the rate of physical weathering from concentrated (i.e. turbulent) flow, supersedes the calcite precipitation rate, thus preventing porosity reduction from secondary mineralization.

Fifth, by comparing peak discharge between sites we see field-scale variability in the maximum amount of recharge that the epikarst is capable of transmitting at any point is time. This is aligned with other similar studies (e.g., Smart and Friederich, 1987; Tooth and Fairchild, 2003) and suggests that variability in peak discharge between stations is controlled by the types of porosity and flow paths that activate in response to variable size recharge events. After periods of significant recharge, drainage systems within the epikarst may reach maximum saturation so that they cannot accommodate any additional flow. In general, drainage systems within the epikarst dominated by higher permeability are able to accommodate higher peak discharges but offer less retention. This is true unless activation of high flow pathways can distribute infiltration to areas of greater storativity.

Sixth, recession analysis has shown that a significant (i.e. up to 50%) portion of recharge can be stored in baseflow reserves. This has significant implications for the regulatory control of karst recharge because longer residence times associated with increased storativity allows for increased soil-rock-water interaction and natural attenuation of surface applied contaminants, whereas quickflow makes the underlying transmission zone particularly susceptible to contamination. Recession coefficients provide further evidence for flow-routing based on the number and permeability type (e.g., matrix, fissures, fractures, and conduits) that are available to accommodate flow at varying discharges. Stations with higher recession coefficients receive flow from higher permeability pathways, such as well-drained conduits and large interconnected fractures. Stations with lower recession coefficients are more capable of storing water in low permeability pathways, such as small fissures, soils, and residuum. Comparison of recession coefficients between stations provides evidence to suggest the degree of structural evolution and

drainage organization in the epikarst. Recession coefficients calculated with two different methods (Tables 3 & 4) reveal differences that suggest clarity of segment identification is lost when using the MRC method, but this method provides a better assessment of overall recession behavior.

A conceptual model of flow and storage in the epikarst over James Cave is shown as Figure 22. The model shows that flow travels along a complex series of low permeability fissures and fractures that come together into higher conductivity fractures and conduits that are enlarged by physical and chemical weathering. Baseflow storage primarily occurs in low permeability compartments (thin lines) and quickflow primarily occurs in high permeability flow paths (thick lines). In Figure 22, we also see that high flow pathways activate based on the amount of recharge received, and we see different types of porosity indicated by "α" (i.e. recession coefficients). Figure 22 also shows differences in epikarst structure and storativity characteristics between drips stations (i.e. field scale variability), suggesting that the epikarst over MS3 is more developed than MS1 and MS2 because it is dominated by higher permeability and lower storativity, except in high order flowpaths that are only used after significant seasonal recharge.

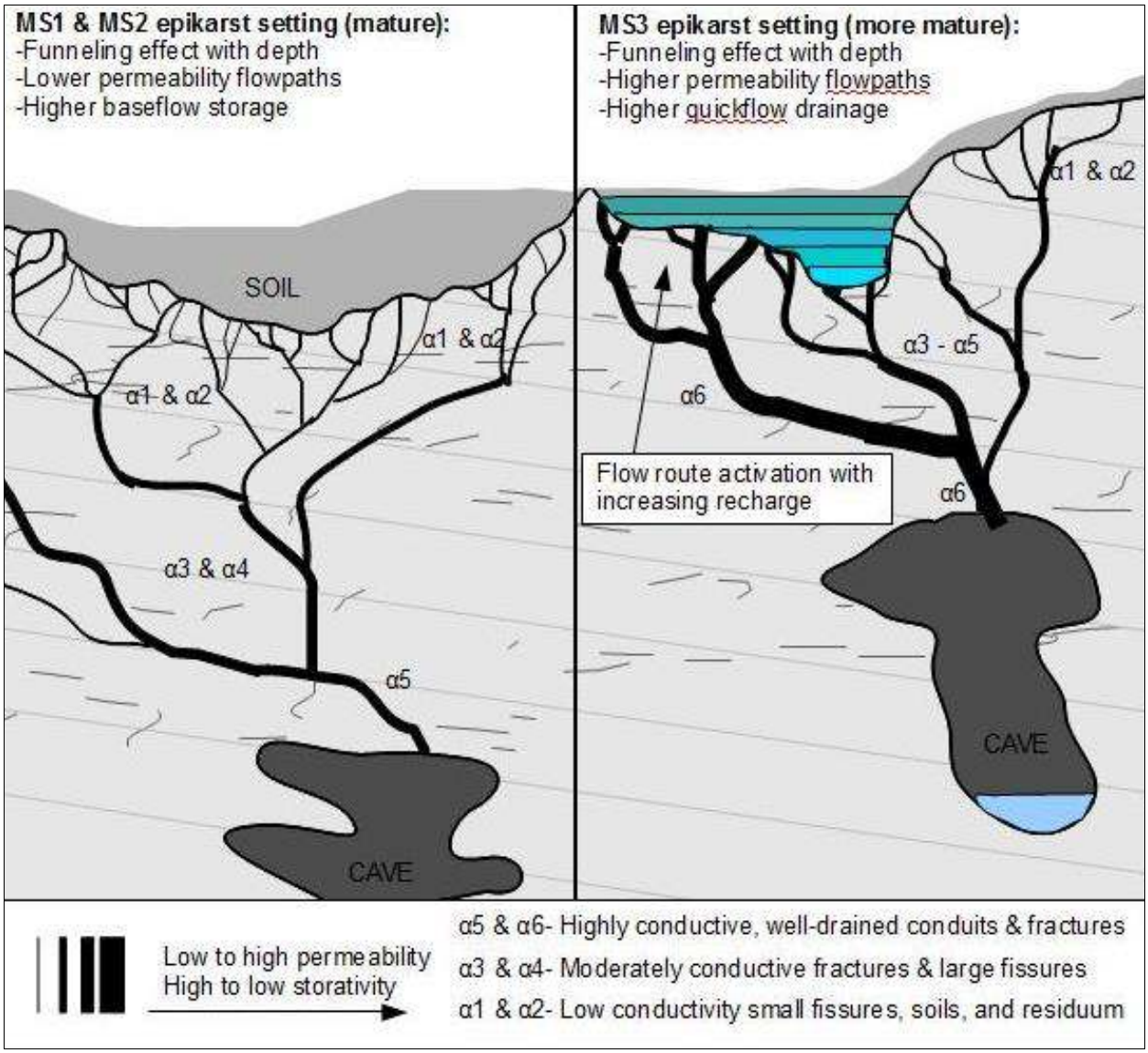

Figure 22. Conceptual model of epikarst flow and storage characteristics at James Cave.

7. CONCLUSIONS

Similar to Bakalowicz (2004), the conceptual model developed in this thesis shows that the epikast serves as the interface between surface environmental change and the hydrologic behavior of a karst aquifer, and as such, the epikarst serves to regulate the quantity and quality of water found in karst aquifers. The main conclusions of this study are:

- Effective recharge in the epikarst occurs seasonally (i.e. winter and spring).

- Flow is funneled down from the ground surface to epikarst flow paths.
- More permeable flow routes offer less storativity and more efficient drainage.
- Additional flow routes and storage compartments activate upon increasing effective recharge.
- Heterogeneities in the epikarst create field-scale variations in epikarst's regulatory control on flow and storage.
- The epikarst can store more than 50% of effective recharge in baseflow compartments.
- Storage is enhanced by epikarst thickness.
- Baseflow storativity in the epikarst supports stream baseflow.

It is expected that although field-scale heterogeneities may complicate epikarst characterization, that in similar karst settings (i.e. Shenandoah Valley karst) we can expect that after significant seasonal recharge, the epikarst can temporarily store a significant portion of recharge in low permeability flow paths that join with depth and focus drips to speleothems. More developed (mature) areas offer less storativity and collect flow from larger contributing drainage areas. This is critical information for quantifying storage capacity and retention time of groundwater reserves, and also for delineating recharge protection zones. Results from this work are intended to aid watershed managers by providing a methodology of different techniques that can be used to quantify important characteristics about the epikarst in order to accommodate increasing demands and improve strategies for water resource management in karst aquifers.

REFERENCES CITED

ASCE-EWRI, 2004, The ASCE Standardized Reference Evapotranspiration Equation: Technical Committee report to the Environmental and Water Resources Institute of the American Society of Civil Engineers from the Task Committee on Standardization of Reference Evapotranspiration, p. 173.

Bakalowicz, M., 2004, The epikarst, the skin of karst: Epikarst, Jones WK, Culver DC and JS Herman (Eds). Shepherdstown, West Virginia, Karst Waters Institute Special Publication 9.

Baker, A., Barnes, W.L., and Smart, P.L., 1997, Variations in the discharge and organic matter content of stalagmite drip waters in Lower Cave, Bristol: *Hydrological Processes*, v. 11, p. 1541-1555.

Baldini, J. U. L., McDermott, F., and Fairchild, I. J., 2006, Spatial variability in cave drip water hydrochemistry: Implications for stalagmite paleoclimate records: Chemical Geology, v. 235, no. 3-4, p. 390-404.

Bartholomew, M., 1987, Structural evolution of the Pulaski thrust system, southwest Virginia: GSA Bulletin, v. 99, no. 4, p. 491-510.

Brahana, V., and Pennington, D., 2010, Is it possible to predictively model shallow karst aquifers at a meaningful scale: Abstracts with Programs- Geological Society of America, v. 42, no. 2, p. 99.

Fairchild, I.J., Tuckwelb, G.W., Bakera, A., and Tooth, A., 2006, Modelling of dripwater hydrology and hydrogeochemistry in a weakly karstified aquifer (Bath, UK): Implications for climate change studies: Journal of Hydrology, v. 321, p. 213-231.

Ford, D., and Williams, P., 2007, Karst Hydrogeology and Geomorphology: John Wiley & Sons, Ltd., p. 45-52, 116, 119, 132-136, 154-163, and 175-191.

Genty, D., and Deflandre, G., 1998, Drip flow variations under a stalactite of the Pere Noel cave Belgium: Evidence of seasonal variations and air pressure constraints: Journal of Hydrology, v. 211, p. 208-232.

Klimchouk, A.B., 2004, Towards defining, delimiting and classifying epikarst: Its origin, processes and variants of geomorphic evolution: Speleogenesis and Evolution of Karst Aquifers. v. 2, no. 1, p. 1-13.

KWI, 2003, What is karst and why is it important? Available from www.karstwaters.org/kwitour/whatiskarst.htm.

Mangin, A., 1975, Contribution a l'etude hydrodynamique des aquiferes karstiques: These Universite de Dijon, p. 124.

Milanovic, P., 1976, Water regime in deep karst. Case study of the Ombla spring drainage area: Karst Hydrology and Water Resources, ed. Yevjevich, Colorado, v. 1, p. 165-191.

Padilla, A., Pulido-Bosch, A., and Mangin, A., 1994, Relative importance of baseflow and quickflow from hydrographs of karst springs: Ground Water, v. 32, no. 2, p. 267-277.

Posavec, K., Parlov, J., and Nakic, Z., 2010, Fully automated objective-based method for Master Recession Curve separation: Ground Water, v. 48, no. 4, p. 598-603.

Schwartz, B.F., and Schreiber, M.E., 2009, Quantifying potential recharge in mantled sinkholes using ERT: Groundwater, v. 47, no. 3, p. 370-381.

Smart, P., and Friederich, H., 1987. Water movement and storage in the unsaturated zone of a maturely karstified carbonate aquifer, Mendip Hills, England; Proceedings of Conference on Environmental Problems in Karst Terranes and their Solutions: National Water Well Association, Dublin, Ohio, p. 59-87.

Snyder, R.L., and Eching, S., 2007, PMday: University of California, Davis, CA. Available from http://biomet.ucdavis.edu/evapotranspiration.html.

Snyder, R.L., and Eching, S., 2009, Penman-Monteith daily (24-hour) Reference Evapotranspiration Equations for Estimating ETo, ETr, and HS ETo with Daily Data: University of California, Davis, CA. Available from http://biomet.ucdavis.edu/evapotranspiration.html.

The Southeast Regional Climate Center, 2010, Historical climate summaries for Virginia. Available from http://www.sercc.com/climateinfo/historical/historical_va.html.

Tooth, A.F., and Fairchild, I.J., 2003, Soil and karst aquifer hydrologic controls on the geochemical evolution of speleothem-forming drip waters, Crag Cave, southwest Ireland: Journal of Hydrology, v. 273, p. 51-68.

Trapp, H., and Horn, M.A., 1997, USGS Ground Water Atlas 730-L. Available from http://pubs.usgs.gov/ha/ha730/ch_l/L-text5.html

University of Virginia Climatology Office, 2010, Virginia Potential Evapotranspiration, Annual Precipitation, and Annual Precipitation Minus Potential Evapotranspiration. Available from http://climate.virginia.edu/va_pet_prec_diff.htm

USDA-NRCS, 2006, Web Soil Survey. Available from http://websoilsurvey.nrcs.usda.gov/app/WebSoilSurvey.aspx.

Vesper, D.J., Loop, C.M., White, W.B., 2000, Contaminant transport in karst aquifers: Theoretical and Applied Karstology, v. 13, p. 63-73.

Virginia Agricultural Experiment Station, 2010, College Farm Weather Data. Available from http://www.vaes.vt.edu/college-farm/weather/index.html

White, W. B., 2002, Karst hydrology: recent developments and open questions: Engineering Geology, v. 65, p. 85-105.

Wikimedia.org, 2009, Pulaski County, Virginia. Available from http://upload.wikimedia.org/wikipedia/commons/

Williams, P.W., 1985, Subcutaneous hydrology and the development of doline and cockpit karst: Zeitschrift fur Geomorphologie, v. 29, no. 4, p. 463-82.

Williams, P., 2008, The role of the epikarst in karst and cave hydrogeology, a review: International Journal of Speleology, v. 37, p. 1-10.